hcp and *fcc* Nickel Nanoparticles Prepared from Organically Functionalized Layered Phyllosilicates of Nickel(II)

Mireille Richard-Plouet,*[,†,‡] Murielle Guillot,[†] Serge Vilminot,[†] Cédric Leuvrey,[†] Claude Estournès,[†,§] and Mohamedally Kurmoo*[,⊥]

IPCMS−GMI, UMR 7504 CNRS-Université Louis Pasteur, 23 rue du Loess, 67034 Strasbourg Cedex, France, Institut des Matériaux Jean Rouxel, UMR 6502 CNRS−Université de Nantes, 2 rue de la Houssinière, BP32229, 44322 Nantes Cedex, France, CIRIMAT, UMR 5085 CNRS−Université Paul Sabatier−Institut National Polytechnique de Toulouse, 118 route de Narbonne, 31062 Toulouse Cedex, France, and Laboratoire de Chimie de Coordination Organique, UMR-7140 CNRS, Université Louis Pasteur, 4 rue Blaise Pascal, 67000 Strasbourg Cedex, France

Received October 23, 2006. Revised Manuscript Received December 7, 2006

We report on the formation of air-stable fcc Ni nanoparticles via the rarely observed metastable hcp Ni from two organically modified layered Ni(II) phyllosilicates at a moderately low temperature of less than 573 K in an inert atmosphere. The presence of hcp Ni as an intermediate is related to the organization of the nickel atoms within the layers of the phyllosilicates, which is a triangular network with Ni−Ni distances of 3.2 Å protected by a strong covalent Si−O network on each surface. Characterizations of the products were performed by TG-DTA coupled to mass spectroscopy, in situ X-ray diffraction, electron microscopy, infrared, and in situ magnetization measurements. TEM shows that the fcc Ni particles are spherical and that the size (average of ca. 20 nm) depends on the starting phyllosilicate. Given that the amount of reduced Ni is proportional to the organic content and not to the Ni content of the phyllosilicates when the atmosphere is inert, we propose that the reduction takes place by the gases produced during the decomposition of the organic moiety. The stabilization of the hcp Ni phase depends on the percentage of Si−O coverage of the surface.

Introduction

The science of nanosized materials is a fast growing area of research due to its wide applicability at every level, from everyday household goods to large-scale industrial plants. Some areas for application include medicine, catalysis, and magnetism.[1,2] At the heart of this field of science lies the elaboration of the nanosized objects of interest. Consequently, there are several well-established chemical and physical approaches for their preparations employing different techniques.[3] Solution,[4−6] sol−gel,[7−9] solid-state,[10−12] as well as particle implantation[13] were adopted. Because magnetism has been our principal interest in the past few years, we have explored different simple and convenient ways of making nanosized magnetic elements and oxides in different matrices starting from different and appropriate precursors,[14] and in one particular case, we have followed on to shaping the nanoparticles by bombardment with heavy ions to increase the coercive field of cobalt implanted in silica on silicon wafer.[15] In particular, we are searching for precursors with the appropriate composition of metal ions as the desired products, for example, the layered-double-hydroxide

* To whom correspondence should be addressed. E-mail: mireille.richard@cnrs-imn.fr (M.R.-P.); kurmoo@chimie.u-strasbg.fr (M.K.). Phone: 00 33 240 37 39 96 (M.R.-P.); 00 33 3 90 24 13 56 (M.K.). Fax: 00 33 240 37 39 95 (M.R.-P.); 00 33 3 90 24 13 25 (M.K.).

† IPCMS−GMI, Université Louis Pasteur.

‡ Institut des Matériaux Jean Rouxel, Université de Nantes.

§ CIRIMAT, Université Paul Sabatier.

⊥ Laboratoire de Chimie de Coordination Organique, Université Louis Pasteur.

(1) *Nanomagnetism*; Hernando, A., Ed.; Kluwer Academic: Dordrecht, The Netherlands, 1993.

(2) Johnson, B. F. G. *Top. Catal.* **2003**, *24*, 147−159.

(3) Cushing, B. L.; Kolesnichenko, V. L.; O'Connor, C. J. *Chem. Rev.* **2004**, *104*, 3893−3946.

(4) Toneguzzo, P.; Viau, G.; Fievet, F. In *Handbook of Advanced Magnetic Materials*; Liu, Y., Sellmyer, D. J., Shindo, D., Eds.; Springer: New York, 2006; Vol. 3, pp 217−266.

(5) Carturan, G.; Cocco, G.; Enzo, S.; Ganzerla, R.; Lenarda, M. *Mater. Lett.* **1988**, *7*, 47−50.

(6) Illy, S.; Tillement, O.; Machizaud, F.; Dubois, J. M.; Massicot, F.; Fort, Y.; Ghanbaja, J. *Philos. Mag.* **1999**, *79*, 1021−1031.

(7) Takahashi, R.; Sato, S.; Sodesawa, T.; Nakamura, N.; Tomiyama, S.; Kosugi, T.; Yoshida, S. *J. Nanosci. Nanotechnol.* **2001**, *1*, 169−176.

(8) Trimmel, G.; Lembacher, C.; Kickelbick, G.; Schubert, U. *New J. Chem.* **2002**, *26*, 759−765.

(9) Goya, G. F.; Fonseca, F. C.; Jardim, R. F.; Muccillo, R.; Carreno, N. L. V.; Longo, E.; Leite, E. R. *J. Appl. Phys.* **2003**, *93*, 6531−6533.

(10) Gerardin, C.; Kostadinova, D.; Sanson, N.; Coq, B.; Tichit, D. *Chem. Mater.* **2005**, *17*, 6473−6478.

(11) Fu, Y.; Zhang, L. *J. Solid State Chem.* **2005**, *178*, 3595−3600.

(12) Li, P.; Liu, J.; Nag, N.; Crozier, P. A. *J. Phys. Chem. B* **2005**, *109*, 13883−13890.

(13) Sze, J. Y.; Tay, B. K.; Pakes, C. I.; Jamieson, D. N.; Prawer, S. *J. Appl. Phys.* **2005**, *98*, 066101/1−3. (b) Cintora-Gonzalez, O.; Estournès, C.; Guille, J. L.; Muller, D.; Grob, J. J. *Nucl. Instrum. Methods Phys. Res., Sect. B* **1999**, *147*, 422−426. (c) Magruder, R. H.; Weeks, R. A.; Zuhr, R. A. J.; Whichard, G. *J. Non-Cryst. Solids* **1991**, *129*, 46−53. (d) Battaglin, G.; Bertoncello, R.; Casarin, M.; Cattaruzza, E.; Mattei, G.; Mazzoldi, P.; Trivillin, F.; Urbani, M. *J. Non-Cryst. Solids* **1999**, *253*, 251−260. (e) Stepanov, A. L.; Hole, D. E.; Townsend, P. D. *Nucl. Instrum. Methods Phys. Res., Sect. B* **2000**, *166−167*, 882−886. (f) Takeda, Y.; Hioki, T.; Motohiro, T.; Noda, S.; Kurauchi, T. *Nucl. Instrum. Methods Phys. Res., Sect. B* **1994**, *91*, 515−519.

(14) Estournès, C.; Lutz, T.; Guille, J. L. *J. Non-Cryst. Solids* **1996**, *197*, 192−196. (b) Estournès, C.; Lutz, T.; Happich, J.; Quaranta, T.; Wissler, P.; Guille, J. L. *J. Magn. Magn. Mater.* **1997**, *173*, 83−92. (c) Schweyer-Tihay, F.; Estournès, C.; Braunstein, P.; Guille, J. L.; Paillaud, J. L.; Richard-Plouet, M.; Rosé, J. *Phys. Chem. Chem. Phys.* **2006**, *8*, 4018−4028.

10.1021/cm062521c CCC: $37.00
Published on Web 01/26/2007

$CoFe_2(OH)_4(CO_3)_2 \cdot nH_2O$ to form $CoFe_2O_4$.[16] The decomposition of solutions of appropriate mixtures of magnetic transition metal ions trapped in cavities of xerogels is a technique that has had wide applications.[8,16] This approach is often used when dispersion of metal nanoparticles is required, in particular, in cases for catalytic reaction to be promoted. However, control of the size distribution and spatial homogeneity remain two big obstacles in this approach. Therefore, we have been looking at the solid-state formation of magnetic nanoparticles using mechanical milling of layered-double-hydroxide with the appropriate metal contents to prepare nanoparticles of $Co_xFe_{3-x}O_4$. Unfortunately, the high-energy ball-milling does not afford full control of the desired characteristics. Here, we present the formation of nickel nanoparticles from a one-step decomposition of organically modified phyllosilicates, $Ni_3Si_{2.13}(C_3H_6NH_3)_{1.98}(O_{5.28},OH_{1.05},F_{0.69})(CH_3COO)_{2.25}.1.76H_2O$, labeled as **S20**, and $Ni_3Si(C_3H_6NH_3)(O_{1.9},OH_{4.45},F_{0.65})(CH_3COO)_{1.1}.0.38H_2O$, labeled as **S50**, in an inert atmosphere at moderately low temperatures. Both of these starting materials have been characterized and were found to exhibit long-range magnetic ordering below 18[17] and 21 K,[18] respectively. The approach presented here and the starting materials used have various advantages over the previous ones. First, the presence of the silicate provides protection to the nanoparticles from oxidation as in xerogels. Second, the layered structure of the silicate provides a better medium for catalysis at the surface of the particles. Third, slow diffusion of the produced metal in the layered silicate results in an even distribution of particles of narrow size distributions. And last, the strong covalent bonding of the silicate species in the phyllosilicate and with the transition metal layer allowed us to evidence the transitory presence of the elusive hcp Ni in a temperature range from 423 to 623 K.

Experimental Section

Synthesis. The phyllosilicates were obtained as described previously by the hydrothermal reaction of nickel acetate tetrahydrate and aminopropyltriethoxysilane. The two silicate starting materials are $Ni_3Si_{2.13}(C_3H_6NH_3)_{1.98}(O_{5.28},OH_{1.05},F_{0.69})(CH_3COO)_{2.25} \cdot 1.76H_2O$, labeled as **S20**,[17] and $Ni_3Si(C_3H_6NH_3)(O_{1.9},OH_{4.45},F_{0.65})(CH_3COO)_{1.1} \cdot 0.38H_2O$, labeled as **S50**.[18] Each can be selectively prepared by choosing the amount of water used during the hydrothermal treatment. For the present study, the as-prepared silicates consisting of fine platelets were dispersed in water and, upon sedimentation, they were restructured as films on different substrates such as glass, metal, MgO, or mica.[19−21] The films can be peeled off the substrate to leave free-standing, highly oriented materials.

Physical Techniques. A preliminary determination of the temperature at which the reduction of Ni^{2+} to Ni^0 starts was performed by in situ magnetization measurements of powdered samples on a Faraday balance ($H = 5.9$ kOe) under a controlled atmosphere of either 5% H_2/N_2 (followed by annealing at 800 K or 1200 K for 2 h) or argon (followed by annealing at 800 K for 1 h).

Isothermal magnetization was measured at 295 K on a Quantum Design MPMS-XL SQUID magnetometer on films deposited on nonmagnetic MgO substrates.

Thermogravimetric (TG) and differential thermal (DT) analyses were performed on powders (ca. 20 mg) of the pure compounds under argon on a SETARAM 92, employing a heating rate of 4 K/min. A prior pumping of the sample chamber was performed in order to remove oxygen that may result in oxidation of the particles. A mass spectrometer coupled to the apparatus was used to monitor the nature and the quantity of gases evolved during the decomposition of the organic moiety.

Infrared spectra were recorded by transmission through thin films deposited on cleaved mica by use of an ATI MATTSON FTIR spectrometer. The spectra were recorded at room temperature after annealing of the films at 573 K for 0, 0.5, 2, 6, and 15 h.

Powder X-ray diffraction (PXRD) patterns were recorded up to 873 K, under vacuum (1×10^{-5} mbar), using an INEL diffractometer equipped with Co−$K_{\alpha 1}$ radiation (1.789 Å) and a curved detector, covering 120° in 2θ. The diffraction peaks were calibrated with those of a silicon powder sample. The heating rate was 5 K/min. Each diffraction pattern was recorded for 0.5 h in increasing step of 50 K. Another experiment was conducted at a fixed temperature of 573 K for a period of 5.5 h. Following the suggestion of one of the referees, we performed another series of experiments in which we have generated the nanoparticles of different samples of **S20** and **S50** in situ at 573 K in a vacuum using an Anton Paar HTK 1200N oven chamber on a high-resolution powder diffractometer (Bruker D8 Advance, $\lambda = 1.5406$ Å) to evidence the formation of nickel with the hexagonal structure.

For electron microscopy, two types of preparation were used. First, the samples were dispersed in alcohol and then deposited on a carbon film, which had previously been sputtered on a copper grid. Second, films were allowed to settle on epoxy resin (Epon) blocks; after drying, they were embedded in another epoxy layer. They were then cut with an ultramicrotome equipped with a diamond knife. The latter preparation allows one to make observation for samples aligned perpendicular to the layers of the silicate. Observations were performed on a TOPCON 002B microscope operating at a 200 kV accelerating voltage.

Results

In situ Magnetization in a 5% H_2/N_2 Atmosphere. Following our previous experiences in the two studies reported on the two starting compounds,[18,19] we proceed in determining the temperature at which the nickel nanoparticles start to form and estimating the amount of nickel produced. These were done by in situ magnetization measurements on an adapted Faraday balance equipped with a controlled reducing atmosphere consisting of 5% H_2 in N_2. The applied field was fixed to 5.9 kOe, and the magnetization measurements as a function of temperature were performed on

(15) D'Orléans, C.; Stoquert, J. P.; Estournès, C.; Cerruti, C.; Grob, J. J.; Guille, J. L.; Haas, F.; Muller, D.; Richard-Plouet, M. *Phys. Rev. B* **2003**, *67*, 220101/1−4. (b) D'Orléans, C.; Stoquert, J. P.; Estournès, C.; Grob, J. J.; Muller, D.; Guille, J. L.; Richard-Plouet, M.; Cerruti, C.; Haas, F. *Nucl. Instrum. Methods Phys. Res., Sect. B* **2004**, *216*, 372−378.

(16) Manova, E.; Kunev, B.; Paneva, D.; Mitov, I.; Petrov, L.; Estournes, C.; D'Orleans, C.; Rehspringer, J-L.; Kurmoo, M. *Chem. Mater.* **2004**, *16*, 5689−5696.

(17) Guillot, M.; Richard-Plouet, M.; Vilminot, S. *J. Mater. Chem.* **2002**, *12*, 851−857.

(18) Richard-Plouet, M.; Vilminot, S.; Guillot, M.; Kurmoo, M. *Chem. Mater.* **2002**, *14*, 3829−3836.

(19) Richard-Plouet, M.; Guillot, M.; Traverse, A.; Chateigner, D.; Vilminot, S. *Nucl. Instrum. Methods Phys. Res., Sect. B* **2003**, *200*, 148−154.

(20) Schlegel, M.; Manceau, A.; Chateigner, D.; Charlet, L. *J. Colloid Interface Sci.* **1999**, *215*, 140−158.

(21) Xu, Z. P.; Stevenson, G. S.; Lu, C.-Q.; Lu, G. Q.; Bartlett, P. F.; Gray, P. P. *J. Am. Chem. Soc.* **2006**, *128*, 36−37.

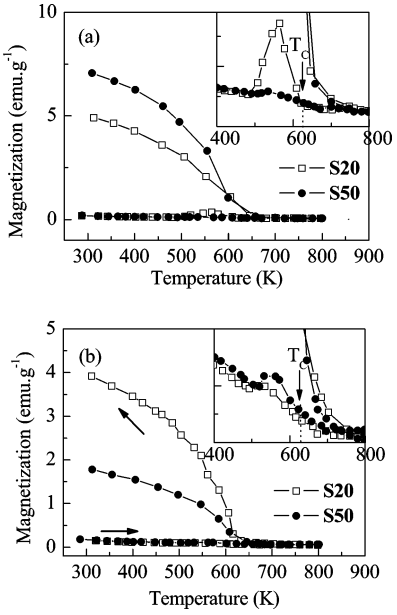

Figure 1. Temperature dependence of the in situ magnetization in an applied field of 5.9 kOe on increasing and decreasing temperature from 298 to 800 K under (a) 5% H_2/N_2 and (b) Argon for **S20** (open squares) and **S50** (filled circles).

warming from 298 to 800 K (Figure 1 a). The precursors are paramagnetic above room-temperature because of the weak near-neighbor interactions between Ni(II) centers, resulting in a decrease in the magnetization from 298 up to 500 K. At 500 K for **S20** and 520 K for **S50**, the magnetization increases to a peak and returns back to being paramagnetic at the Curie temperature of nickel ($T_C = 627$ K).[22] Upon subsequent cooling of the sample in the same field, following annealing at 800 K for 1 h, the magnetization starts to increase smoothly from 627 K to room temperature. Taking into account that the silicates initially contain 28 wt % (**S20**) and 39 wt % (**S50**) Ni^{2+} and the saturation magnetization of bulk Ni metal is 55 emu g^{-1}, we estimate 32% (**S20**) and 33% (**S50**) reduction of Ni^{2+} in the silicates from the values of magnetization of 4.9 emu g^{-1} (**S20**) and 7 emu g^{-1} (**S50**) at room temperature (Figure 1a). When annealing is performed at 1200 K, the amount of reduced Ni is higher (Figure S1, Supporting Information), 72 and 82%, respectively, for **S20** and **S50**. After this thermal treatment, the metal aggregates appear as submicrometer particles together with silica grains containing the remaining Ni^{2+} and possibly small nonmagnetic Ni clusters. Because of the highly reducing atmosphere of hydrogen, the reduction is quite rapid and thus results in metal particles that are agglomerated into 100 nm clusters, i.e., much bigger than the ones observed after thermal treatment under an argon atmosphere (see below). This suggests a higher mobility of the metal in a H_2/N_2 atmosphere at this high temperature.

In situ Magnetization in an Argon Atmosphere. Under an argon atmosphere, the basic features of the temperature dependence of the magnetization are similar to those under hydrogen, concerning the temperature of the events. The reduction begins at almost the same temperatures as in H_2,

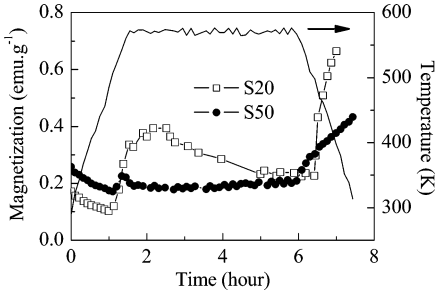

Figure 2. Time dependence of the in situ magnetization in an applied field of 10 kOe from 298 to 573 K followed by annealing for 5.5 h for **S20** (open squares) and **S50** (filled circles).

that is 508 and 523 K for **S20** and **S50,** respectively (Figure 1b). The magnetization after cooling from 800 K to room temperature is close to 3.9 emu g^{-1} for **S20**, which corresponds to only 25% of the Ni^{2+} being reduced. For **S50**, the magnetization after cooling to room temperature reaches 1.8 emu g^{-1}, corresponding to even less Ni^{2+} reduced, 8%. The fact that the bifurcation in the magnetization is at the Curie temperature of bulk metallic nickel rules out the possible formation of the metastable Ni_3C at lower temperatures, given that the Ni_3C is magnetic below 627 K.[22] It is also worth pointing out that the transformation of Ni_3C to Ni is above 723 K.[23] Thus, one should not observe a sharp peak in the magnetization on warming at ca. 550 K (see inserts of Figure 1).

From the above observations, we note that the amount of reduced nickel is proportional to the original composition if the reduction is performed in H_2/N_2, whereas it is proportional to the organic content when the reduction is performed in vacuum or argon. Given that the reaction is dynamic because of the movement of the nickel atoms inside the silicate and is especially slow at this low temperature, we studied the production of the reduced metal as a function of time. In this experiment, we measured the evolution of the magnetization with time in an applied field of 10 kOe while keeping the sample at 573 K (Figure 2), a temperature just above the beginning of the reduction and below the Curie temperature of nickel. Therefore, the measurement was performed while the sample was heated to 573 K at a rate of 3 K/min and subsequently, annealed at 573 K for 4.5 h. For both samples, the reduction begins at 500 K. For **S20**, the magnetization reaches a maximum after 0.5 h at 573 K, followed by a slow decrease. In contrast, for **S50**, a peak appears after a few minutes followed by a marginal increase during the annealing at 573 K. As a time evolution is detected, further characterizations have been performed on samples heat-treated at 573 K for different periods of time up to 15 h by measuring the isothermal magnetization at 295 K on a SQUID magnetometer. Figure 3 presents the magnetization versus applied field for samples annealed for 0.5, 2, 6, and 15 h. For **S20**, the quantity of reduced Ni increases with the annealing time, as expected for a progressive thermal reduction process and the slow dynamics in the dense silicate matrix. For **S50**, we observe less Ni^{2+} reduction and a decrease in the saturation magnetization for the 15 h

(22) Kittel, C. *Physique de l'état Solide*, 5th ed.: Bordas: Paris, 1983; p 465.

(23) Leslie-Pelecky, D. L.; Zhang, X. Q.; Kim, S. H.; Bonder, M.; Rieke, R. D. *Chem. Mater.* **1998**, *10*, 164−171.

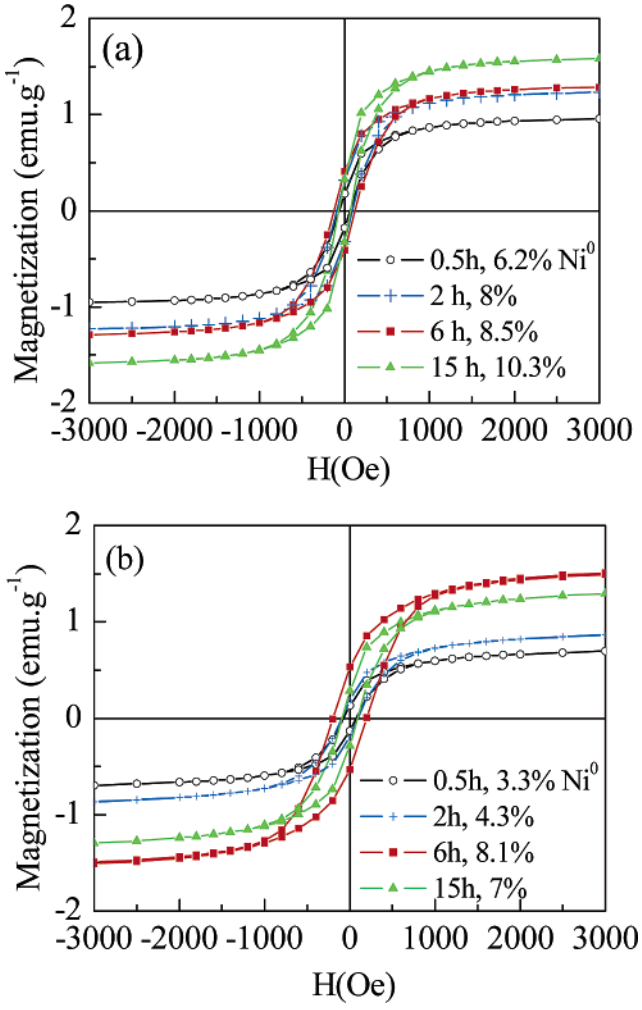

Figure 3. Isothermal magnetization at 295 K on films of (a) **S20** and (b) **S50** annealed in argon at 573 K for different periods of 0.5, 2, 6, and 15 h.

sample compared to that for 6 h, whereas it continuously increases between 0.5 and 6 h. The coercive field ranges from 50 to 200 Oe, the largest value being observed after 6 h thermal treatment. The results of the thermal treatment under argon indicate that the reduction of Ni^{2+} to metallic particles is only partial and is related to the amount of organic species present in the starting materials. This leads us to propose that the reduction is assisted by the gases such as carbon monoxide produced by the decomposition of the organic. To verify this hypothesis, we looked at the origin of this reduction by a coupled mass spectroscopy with TG-DTA.

Thermogravimetric and Differential Thermal Analyses. TG-DTA was performed under argon from 293 to 1200 K at a rate of 4 K/min with an intermediate plateau of 2 h at 573 K while recording the mass spectrum every 2 min. The two silicates exhibit very similar behaviors; we focus on the **S20** results (Figure 4). **S20** presents two endothermic steps at 473 and 573 K and two others, also endothermic, after the plateau, close to 673 and 723 K. The TGA curve reveals the corresponding steps of weight loss, the major one (ca. 35%) taking place after the 573 K plateau. On the mass spectrometer traces, the volatile products of decomposition below 573 K are associated with m/z (m = mass, z = charge) of 44, 43, 16, and 60, corresponding to carbon dioxide, CH_3-

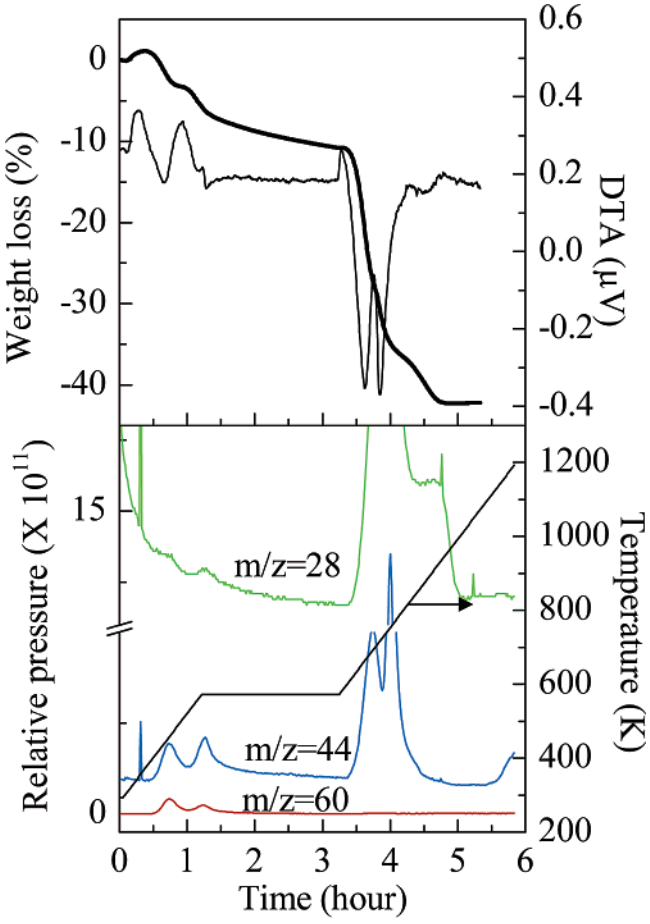

Figure 4. TG-DTA coupled to mass spectroscopy under Ar for **S20** (see text for details). Top: weight loss (thick line), DTA (thin line). Bottom: $m/z = 28$, green; $m/z = 44$, blue; $m/z = 60$, red; temperature program applied to the sample (black line).

CO, methane, and acetic acid, respectively. At temperatures above 573 K, the fragments have 44 and 28 m/z. The latter can be attributed to CO. Other fragments corresponding to the aminopropyl group (such as 85 ± 1 m/z, which can be due to $Si(CH_2)_3NH_x$) are also detected. Smaller fragments such as NH_3 (m/z = 17) and ketene (CH_2, m/z = 14) are also detected. These results confirm TG-DTA observations under an air atmosphere previously reported,[17] where only 15% of the acetate decomposes below 520 K, whereas the rest decomposes together with the aminopropyl group above 520 K. The presence of two endotherms can be related to the decomposition of acetate and aminopropyl groups. PXRD pattern recorded on the TGA residue reveals the presence of fcc Ni metal as sharp Bragg reflections. The TEM image is evidence of the presence of nanometer-sized particles, averaging 15 nm in the body and 3 nm at the edges (see Figure S2 in the Supporting Information).

Infrared Spectroscopy. This study was performed by transmission through films deposited on mica for different annealing times under argon corresponding to the magnetic study presented earlier. In principle, we monitor the changes in the vibrational bands of the organic part associated with the annealing. Figure 5 shows the results obtained for **S20**. Those of **S50** are similar. Considering first the 3400−2800 cm^{-1} region, the bands at 2930 and 2875 cm^{-1} correspond to the stretching vibrations (antisymmetric and symmetric, respectively) of the C−H bond. When the time increases,

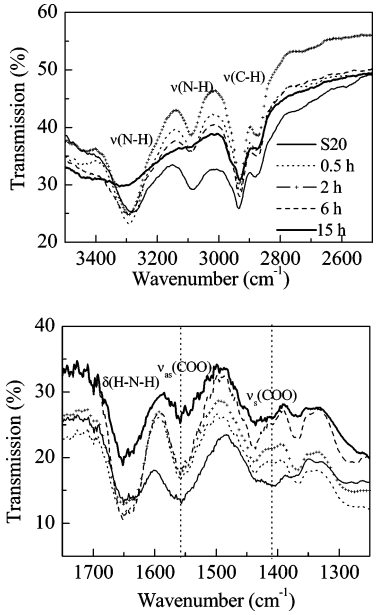

Figure 5. Transmission infrared spectra, recorded at RT, on films of **S20** annealed in argon at 573 K for 0, 0.5, 2, 6, and 15 h.

these bands appear nearly constant even if a small decrease is evident. It is not the case for the band at 3085 cm^{-1}, related to the presence of a NH_3^+ group, whose intensity continuously decreases with annealing time and disappears after 15 h. For the stretching vibration of the N−H bonds (3290 cm^{-1}), its intensity remains constant up to 6 h and decreases for 15 h. The same conclusion can be drawn for the bands in the range 1700−1300 cm^{-1}. Here, the band at 1650 cm^{-1} can be taken as reference (deformation band of $N-H_3$). Again, its intensity is constant up to 6 h and decreases for 15 h. The intensity of the vibration bands at 1550 and 1406 cm^{-1}, associated with the acetate ions, decrease gradually and, in particular, the 1406 cm^{-1} band disappears after 6 h annealing. The bands located at 1430 and 1360 cm^{-1} are attributed to the deformation and wagging vibrations, respectively, of CH_2 groups belonging to the $Si(CH_2)_3NH_3$ species. This is in agreement with the TGA experiment in which the decomposition of acetate ions takes place at a lower temperature than the decomposition of amine. In particular, as the TGA measurements were performed under dynamic conditions, the decomposition temperature of the amine is at 400−450 °C. The annealing process performed in a static mode reveals a lower temperature (300 °C for 15 h).

Temperature Dependence of the X-ray Diffraction under a Vacuum. The PXRD patterns recorded on a conventional powder diffractometer reveal a higher crystallinity for **S50** than **S20** (see Figure S3 in the Supporting Information). It appears that the coherence along the *c*-axis is less for **S20**. At room temperature, the silicates are characterized by two sets of Bragg reflections; the strong, evenly spaced peaks at low angles are attributed to (00*l*), $l = 3, 4, 5, 6$, reflections and the sharp ones at 2.67 and 1.55 Å to (*hk*0). To study the temperature dependence of the PXRD, we used a multidetector diffractometer, which allows reliable data for angles above 10°. Both silicates were therefore heated from 293 to 873 K in a vacuum. Figure 6 presents the PXRD patterns obtained for **S20** and **S50**. There

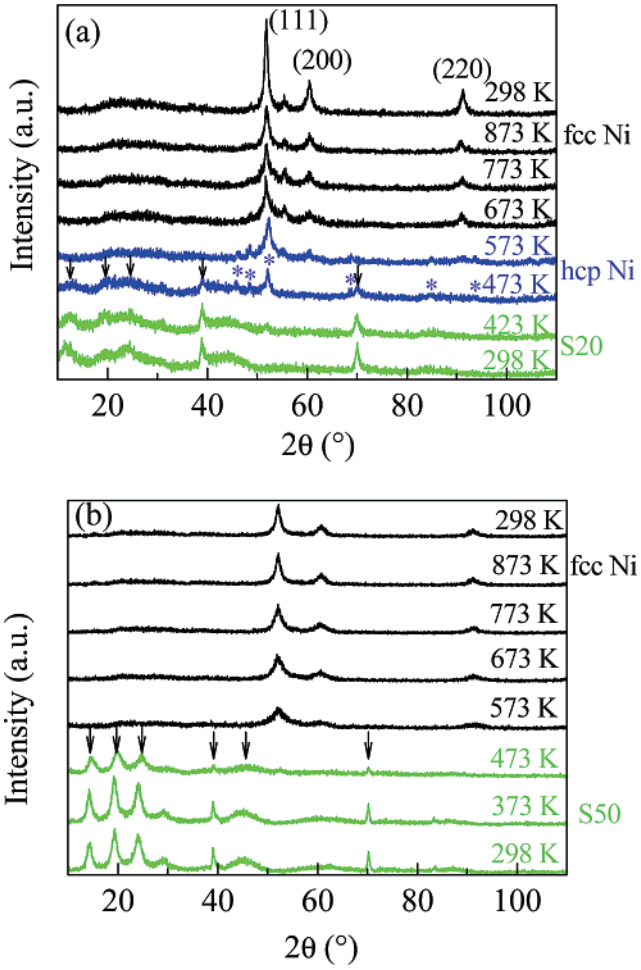

Figure 6. Evolution of the X-ray diffraction patterns with temperature from 298 to 873 K under a vacuum for (a) **S20** and (b) **S50**; arrows and stars indicate X-ray diffraction peaks of the initial silicate and hcp Ni, respectively.

is a lowering of the intensities and a broadening of all reflections as the temperature is increased. For **S20**, a striking transformation starts to take place at 423 K where new peaks appear in the PXRD, the most intense being at 51.9° (d = 2.034 Å). This peak and others (45.8, 48.4, 68.5, 84.7, 93.4, 103.9, 107.1° corresponding to *d*-spacing of 2.299, 2.181, 2.034, 1.586, 1.327, 1.229, 1.134, 1.112 Å) increase in intensities until a temperature of 523 K. Every observed Bragg peaks in this temperature region was indexed to those expected for a hexagonal close packing of nickel (hcp Ni), JCPDS 45-1027, corresponding to (010), (002), (011), (012), (110), (103), (112), and (201), respectively. At higher temperatures, their intensities decrease, followed by a displacement in angle of the peak at 51.9° due to the appearance of a novel peak at 51.8°. The latter and two other peaks gain in intensity as the temperature increases. These three peaks correspond to those of fcc Ni, which is the sole product above 623 K. For **S50**, a similar but less pronounced transformation takes place. The range of temperature for the stability of the intermediate phase, hcp Ni, is the same. At 473 K, a broad peak appears at 51.9° (d = 2.034 Å), corresponding to the (011) reflection of hcp Ni. The other peaks are detectable only when the accumulation time is increased (see next paragraph). At higher temperatures, the three peaks characteristics of fcc Ni become more pro-

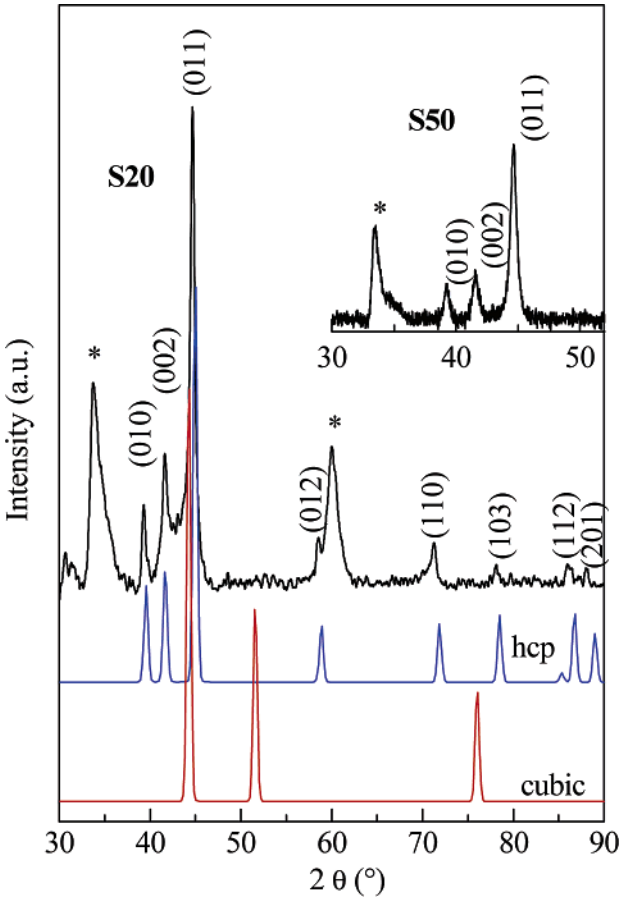

Figure 7. X-ray diffraction pattern of sample **S20** annealed under a vacuum for 1 h at 573 K, the calculated patterns of hcp Ni and fcc Ni are plotted for comparison. Inset: part of the X-ray diffraction pattern of sample **S50** under the same conditions. * indicates the (hk0) reflections of the silicates.

nounced: (111) at 51.8° (2.045 Å), (200) at 62.5°, (1.762 Å) and (220) at 94.3°, (1.246 Å) (PDF file 88-2326). The rather broad peaks indicate that the particles are small. The coherent crystalline domain length evaluated using the Scherrer formula leads to values of less than 10 nm.

To confirm the above observation, we treated different samples in situ at 573 K under a vacuum for 1 h and recorded their diffraction patterns on a high-resolution diffractometer at room temperature. Figure 7 shows the results for an **S20** sample and the theoretical patterns for hexagonal and cubic nickel. In the inset, the result for an **S50** sample for the 3 major peaks is shown. To check the stability of hcp Ni, we undertook a complementary experiment where the sample was heated slowly to 573 K under a vacuum followed by annealing for 5.5 h (see Figure S4 in the Supporting Information). Only the peaks corresponding to hcp Ni are present for the first hour of the annealing process and then both varieties (hexagonal and cubic) coexist for a further 1.5 h. After 3 h annealing, only fcc Ni is detectable. On returning to room temperature, the X-ray diffraction pattern is typical of fcc Ni, indicating rather stable nanoparticles of metallic nickel, which is highly likely to be due to their protection by the silicate layer.

Electron Microscopy. TEM through the platelets in argon shows a homogeneous distribution of spherical particles, indicating a constant dynamics of nickel atoms diffusing through the silica layers during the decomposition process.

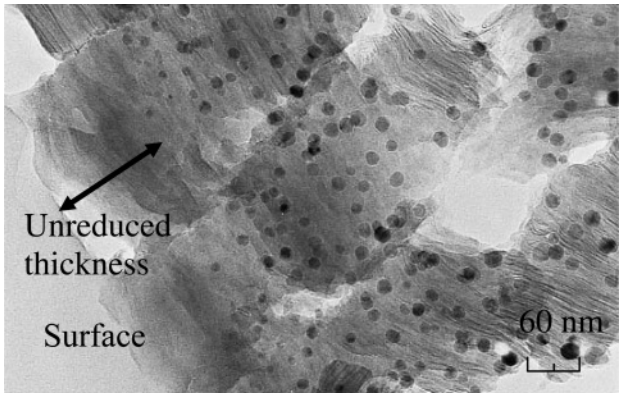

Figure 8. Cross-sectional view of a film annealed under Ar at 573 K for 2 h.

However, when performed on a cross-section of a film (Figure 8), TEM shows two regions. The surface region of the film (ca. 150 nm) is particle-free, and in the body of the film, the particles are evenly distributed. It also indicates that the surface region may be amorphous and the bulk retains the lamellar structure. This view allows us to check the relative homogeneity in the repartition and the size of the particles. For **S20**, the average particle size is smaller than for **S50**. The distribution is relatively narrow and lies in the range 17−23 nm for **S20** and 20−34 nm for **S50** and remains almost constant with time up to 15 h at 573 K. Size distributions performed on **S20** annealed under argon for 0.5, 6, and 15 h are supplied in the Supporting Information (Figure S5). The distribution is centered on 15, 17, and 23 nm, respectively, for the different annealing durations.

Discussion

The formation of nanoparticles of nickel from the organically modified Ni(II) phyllosilicates presents some advantage over other techniques used. It is reasonably cheap and convenient with regards to the low temperatures used and the ease with which the starting materials are available. Furthermore, it needs no additional reducing atmosphere, like hydrogen, for which considerable precautions are required.

A question of technical importance for applications in catalysis and also in magnetism is the even distribution of sizes. The size of the particles appears to be controllable by the temperature at which the reduction is performed and the annealing time. However, the distribution is very good because of the slow dynamics of the elemental nickel produced by reduction in the silica. Furthermore, the stability of the formed particles is very high because of the protection by the silica layers. One drawback of the approach is the low yield of particles compared to when the reduction is performed in 5% H_2/ N_2.

Under the condition of the thermal treatment of **S20** and **S50** under an inert atmosphere, the reducing agents are generated in situ by the decomposition of the organic components. Given the different nature of bonding of the acetate and the propylammonium, their decompositions take place at different temperatures. According to TGA coupled to mass spectroscopy, CO_2 (44 *m*/*z*) and CH_3COOH (60 *m*/*z*) are the two volatile compounds detected below 573 K. This

is in agreement with mass spectrometry results obtained during the thermal decomposition of Ni acetate under a He atmosphere.[24] Carbon dioxide is indeed the main product detected during thermal decomposition of Ni acetate tetrahydrate in helium.

IR spectroscopy as a function of temperature and time also confirms the disappearance of acetate groups with concomitant transformation of NH_3^+ into NH_2. Therefore, two processes can be invoked. First, acetic acid is formed that can either be evacuated or decomposed into CO, source of the reduction process, subsequently evacuated as CO_2. Second, NH_2 is formed by the capture of its proton by the acetate ion; the amino group then acts as the reducing species as in the case of hydrazine. It is quite difficult to differentiate between the two processes. However, these considerations can explain several of the observed phenomena as well as the differences between the two samples, **S20** and **S50**.

The main difference in behavior between the silicates concerns the amount of organic species and the Ni contents; there are twice as many organic species in **S20** compared to **S50**. Assuming the amount of reducing agent is proportional to the organic content, one expects a proportional metallic nickel content after thermal treatment at the same maximal temperature (800 K). Therefore, as the organic content increases on going from **S50** to **S20**, the amount of metallic Ni, estimated from the in situ magnetization measurements on the Faraday balance, produced under similar conditions indeed increases, viz 8% for **S50** and 25% for **S20** (Figure 2). The higher organic content of **S20** can also be invoked to explain the upturn of the magnetization starting at ca. 500 K. The same observation is true for different annealing times at 573 K where SQUID measurements reveal a higher metallic content for **S20** compared to **S50** (Figure 3). Increasing the annealing time to 15 h for **S50** appears to promote the formation of a nonmagnetic component that we believe is the oxidation of the particles to NiO.

The presence of an amorphous surface in the films (ca. 150 nm) and the absence of metallic particles in this region is a second important clue to the reduction coming from decomposition products of the organic. This is due to the escape of the reducing products before reaction can take place. In contrast, the trapped reducing products within the body of the films results in an even and narrow distribution of particles. The smaller average particle size for **S20** is in agreement with the rate at which the particles are formed, which is related to the amount of organic material in the starting solid. The segregation of the nickel from the silicate layer may be the reason why the layered structure of the silicate is still observable in the inner part of the films. On the other hand, the departure of some of the organics within the skin renders it amorphous.

The existence of hcp Ni is rare; it was observed in films obtained by sputtering under hydrogen or nitrogen or by electrolytic processes.[25] Recent examples of the synthesis of hcp Ni are chemical reduction of nickel salts by sodium hydride in butanol[6] and the decomposition of Ni(acetylacetonate)$_2$ in tetrahydrofuran in the presence of a K/B alloy.[5] Hydrazine can also be used as reducing agent in tetrahydrofuran at moderated temperatures.[26] Potassium borohydride induces the reduction of nickel chloride in ethylenediamine at 573 K.[27] Thermolysis at 523 K of Ni formate in an ionic liquid can also lead to hcp Ni particles.[28] A mixture of hcp and fcc Ni particles could be obtained by refluxing Ni acetate in a polyol medium.[29] In these powdered samples, the magnetization at room temperature for hcp Ni is generally found to be lower than that of fcc Ni. This observation seems to be in disagreement with calculations that indicate that the saturation magnetization of hcp Ni is 1.5 times larger than that of fcc Ni.[30] In our case, when the magnetization is recorded in situ while the sample is heated under a flow of argon (Figure 2), we first observe a lowering of the magnetization during the formation of hcp Ni and an increase during its transformation into fcc Ni. These observations agree with the other experimental works. Further work will be needed to elucidate the behavior in the magnetization of bulk and nanosized hcp Ni.

Conclusion

Thermal decomposition of organically modified Ni(II) phyllosilicates under an inert atmosphere produced high spatially ordered and evenly distributed fcc Ni nanoparticles. The reduction to the metallic state is afforded by the in situ production of the reducing components from the decomposition of the organics. Surprisingly, because of the structural nature of the starting materials, which adopt the phyllosilicate structure, and the strong covalent silica layers on the surface, the rare stabilization of the hcp Ni phase has been observed in a narrow range of temperatures. This approach proved to be a simple and convenient way to generate nanoparticles of metals as well as control the size distributions, even density, and dispersion of particles.

Acknowledgment. This work was funded by the "Centre National de la Recherche Scientifique'"(CNRS), France. We are indebted to Gaby Ehret for preparation of cross sections by ultramicrotomy. Vincent Fernandez, Jonathan Hamon, and Pierre-Emmanuel Petit are thanked for their help in XPS and X-ray diffraction.

Supporting Information Available: Temperature dependence of in situ magnetization, various X-ray diffraction patterns, and size distributions. This material is available free of charge via the Internet at http://pubs.acs.org.

CM062521C

(24) de Jesus, J. C.; Gonzalez, I.; Quevedo, A.; Puerta, T. *J. Mol. Catal. A: Chem.* **2005**, *228*, 283−291.
(25) Pascal, P. *Nouveau Traité de Chimie Minérale*, Cobalt-Nickel, 2nd fascicule; Masson et Cie: Paris, 1963; tome XVII, pp 575−577.
(26) Jeon, Y. T.; Moon, J. Y.; Lee, G. H.; Park, J.; Chang, Y. *J. Phys. Chem. B* **2006**, *110*, 1187−1191.
(27) Mi, Y.; Yuan, D.; Liu, Y.; Zhang, J.; Xiao, Y. *Mater. Chem. Phys.* **2005**, *89*, 359−361.
(28) Zhang, S. M.; Zhang, C. L.; Wu, Z. S.; Zhang, Z. J.; Dang, H. X.; Liu, W. M; Xue, Q. J. *Acta Chim. Sin.* **2004**, *62* (15), 1443−1446.
(29) Hinotsu, T.; Jeyadevan, B.; Chinnasamy, C. N.; Shinoda, K.; Tohji, K. *J. Appl. Phys.* **2004**, *95*, 7477−7479. (b) Chinnasamy, C. N.; Jeyadevan, B.; Shinoda, K.; Tohji, K.; Narayanasamy, A.; Sato, K.; Hisano, S. *J. Appl. Phys.* **2005**, *97*,10J309/1−3.
(30) Papaconstantopoulos, D. A.; Fry, J. L.; Brener, N. E. *Phys. Rev. B* **1989**, *39*, 2526−2528.